THE JOURNAL OF PHYSICAL CHEMISTRY B
A JOURNAL OF THE AMERICAN CHEMICAL SOCIETY

pubs.acs.org/JPCB

Article

An Investigation into the Transdermal Behavior of Active Ingredients by Combination of Experiments and Multiscale Simulations

Qi Duan,[‖] Zhicheng Ye,[‖] Kangfu Zhou,[*] Feifei Wang, Cheng Lian, Yazhuo Shang,[*] and Honglai Liu

Cite This: *J. Phys. Chem. B* 2024, 128, 6327−6337

Read Online

ACCESS | Metrics & More | Article Recommendations

ABSTRACT: Transdermal behavior is a critical aspect of studying delivery systems and evaluating the efficacy of cosmetics. However, existing methods face challenges such as lengthy experiments, high cost, and limited model accuracy. Therefore, developing accurate transdermal models is essential for formulation development and effectiveness assessment. In this study, we developed a multiscale model to describe the transdermal behavior of active ingredients in the stratum corneum. Molecular dynamics simulations were used to construct lipid bilayers and determine the diffusion coefficients of active ingredients in different regions of these bilayers. These diffusion coefficients were integrated into a multilayer lipid pathway model using finite element simulations. The simulation results were in close agreement with our experimental results for three active ingredients (mandelic acid (MAN), nicotinamide (NIC), and pyruvic acid (PYR)), demonstrating the effectiveness of our multiscale model. This research provides valuable insights for advancing transdermal delivery methods.

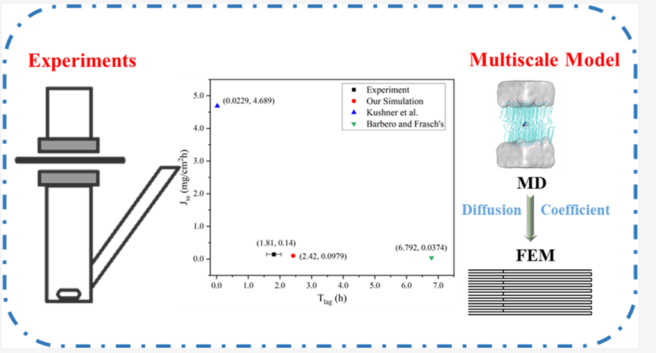

1. INTRODUCTION

The stratum corneum (SC) is the outermost layer of human skin,[1] with a thickness of 10−20 μm,[2] making it highly resistant to external factors such as UV rays and pathogens[3] and, thus, the most difficult to penetrate.[4] Corneocytes are embedded in a lipid matrix to form a "brick-and-mortar" structure".[5] There are two repeating units in the SC. The short periodicity phase (SPP) has a repeat distance of approximately 6 nm, and the long periodicity phase (LPP) has a repeat distance of 13 nm. The unique structure of the stratum corneum imparts significant resistance to penetration, and LPP is assumed to play a key role in the cutaneous barrier function.[6] The study of transdermal behavior is essential in many fields, such as transdermal drug delivery[7] and transdermal absorption of cosmetic active ingredients.[8] When compared to conventional oral or intravenous routes, the transdermal route offers numerous advantages, allowing for noninvasive, painless, and continuous dosing with fewer side effects and greater patient compliance. The skin barrier serves as the limiting factor for transdermal behavior, making it crucial to assess the skin permeability of chemicals.

Currently, the primary method for investigating drug skin permeability is through in vivo/in vitro testing. However, these tests are costly and time-consuming, and the data is susceptible to variations in experimental procedures, skin types, and differences between laboratories.[9,10] Different types of skin, including PAMPA membrane, porcine skin, rat skin, and human skin, exhibit significant differences in permeability.[11,12] Results of experiments on the permeation of 2-phenoxyethanol (PE) indicate that the PAMPA membrane has much higher permeability compared to others. The permeation rates of porcine and rat skin are higher than human skin. Hence, it is crucial to create an efficient and accurate theoretical computational skin model for transdermal behavior to predict the permeability of active ingredients through the skin.

In the previous study, Kushner's research group proposed a two-tortuosity model based on first principles, which illustrated the influence of the branching and lateral diffusion of the lipid pathway on transdermal delivery.[13] They obtained analytical solutions for diffusion flux and cumulative release and successfully predicted the cumulative release profile of naphthol and testosterone. Analytical solutions can provide accurate calculation results for transdermal behavior, but they are difficult to describe complex situations and require the assumption of skin homogeneity, which may affect the

Received: February 2, 2024
Revised: June 9, 2024
Accepted: June 11, 2024
Published: June 24, 2024

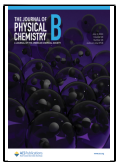

https://doi.org/10.1021/acs.jpcb.4c00735
J. Phys. Chem. B 2024, 128, 6327−6337

accuracy of the calculation results. Cronin et al. developed quantitative structure-permeability relationships (QSPRs) by examining the permeation coefficients of 114 compounds through excised human skin.[14] They observed that the hydrophilicity and relative molecular weight of the active ingredients had a substantial impact on their permeation coefficients. However, the accuracy of QSPR models is limited by the training data set and model assumptions. These two models above do not reflect the molecular-level mechanisms involved in transdermal behavior, and they also ignore the heterogeneity of intercellular lipids.

Intercellular lipids are anisotropic,[15] which may affect the transdermal behavior of active ingredients through the stratum corneum. The diffusion of ingredients in lipids can be divided into lateral diffusion (*xy*-direction) and vertical diffusion (*z*-direction). Wang established a power-law relationship between the lateral diffusion coefficient of lipids $D_{\text{lip-}xy}$ and the molecular weight (MW) based on the diffusion behavior of six kinds of compounds in lipids[16] (see formula 1). Barbero and Frasch also directly used this empirical formula in their studies.[15]

$$D_{\text{lip-}xy} = (1.24 \times 10^{-7}\text{cm}^2/\text{s})\left(\frac{100}{\text{MW}}\right)^{2.43} + (2.34 \times 10^{-9}\text{cm}^2/\text{s}) \quad (1)$$

Although empirical formulas simplify the determination of lipid lateral diffusion coefficients, they lack theoretical support at the microscopic scale. At the microscale, the lipid bilayer is composed of ceramides (CER), cholesterol (CHOL), and free fatty acids (FFA) of equal molar ratio.[17] Ceramides, which comprise approximately 50% of the lipid mass, are molecules containing numerous subclasses,[6] consisting of a sphingosine backbone and a fatty acid chain.[18] Ceramides mainly affect the properties and structure of the lipid matrix in the stratum corneum.[19] They maintain the barrier function of the human epidermis, promote self-repair of the epidermis, maintain long-term self-renewal of the epidermis, and promote the stability of the body's internal environment.[20] Multiple lipid bilayers are stacked to form intercellular lipids.

Based on the SC lipid composition and biophysical and nanoscale information on lipid organization, many different molecular dynamics (MD) simulation models have been proposed to describe the LPP and SPP of the SC lipid matrix. Although molecular dynamics simulations can provide a deeper understanding of the lipid microstructure and assess the diffusion of small molecules within it, they still have some limitations. Das et al. have calculated the excess chemical potential profile and diffusivity for water in one single CER: CHOL: FFA (2:2:1) bilayer by atomistic molecular dynamics simulations. The experimental results for permeability on mammalian skin sections, however, were about 30 times higher than the simulation results.[21] Gupta's team calculated the permeability coefficients of multiple ingredients using molecular dynamics simulations. However, their results were inconsistent with experimental findings as they showed that DMSO and ethanol did not enhance permeability.[22] Therefore, it is difficult to describe the permeation properties of active ingredients by using only molecular dynamics simulations. The study of transdermal behavior requires simulations at multiple scales.

In the current research on transdermal behavior, molecular dynamics simulations mainly focused on the diffusion and permeation coefficient of ingredients and the energy barriers for passing through the bilayer.[23] Finite element simulations were used to calculate some parameters such as the diffusion flux and cumulative release at the bottom of the stratum corneum.[15] It was uncommon for these two simulation scales to be combined to analyze how active ingredients pass through the stratum corneum. Rim et al. first calculated the microscopic diffusion coefficient of ingredients within the lipid bilayer. They considered the stratum corneum homogeneous to calculate the macroscopic diffusion coefficient, which was applied in the finite element simulation. However, the authors used CHOL and DMPC in an equimolar ratio to construct the lipid bilayer, which differs significantly from the actual lipid bilayer structure.[24] Gajula et al. built the lipid bilayer structure using CER, CHOL, and FFA. They calculated the diffusion coefficient of ingredients at different positions in the *z*-direction within the stratum corneum, selecting the results obtained from the center region of the lipid bilayer. They also constructed a lipid pathway model for the stratum corneum and incorporated the diffusion coefficient obtained from molecular dynamics simulations into the finite element model. However, the lipid bilayer is anisotropic and has varying diffusion behavior at different positions.[25] Therefore, we consider both the anisotropic properties of lipids and variations in diffusion coefficients across the bilayer.

Generally, current molecular simulations fail to accurately predict permeability compared to experimental results. Likewise, finite element simulations lack explanations for micromechanisms, while multiscale simulations do not consider lipid anisotropy. Here, we developed a model that incorporates microscopic diffusion processes and examines lipid heterogeneity, which provided a more accurate description of the diffusion of active ingredients in the stratum corneum. Mandelic acid, niacinamide, and pyruvic acid were studied as cases. These are active ingredients that have garnered significant attention due to their unique biochemical properties. These substances exhibit notable antioxidant capabilities,[26] effectively neutralizing free radicals induced by UVB radiation,[27] thereby alleviating skin inflammation and cellular damage.[28] These active ingredients safeguard the skin from UVB-induced harm through mechanisms such as antioxidant action, free radical scavenging, and inflammation regulation, offering potential solutions for skin repair.

In this study, we presented a novel approach for predicting the permeability of active ingredients through the stratum corneum by combining molecular dynamics simulations with finite element methods. Molecular dynamics simulations were used to construct the lipid bilayer structure. The diffusion coefficients of active ingredients in the headgroup and center regions were obtained in different directions via Einstein and Green−Kubo relations. Afterward, we constructed a finite element model of the stratum corneum consisting of stacked corneocytes and intercellular lipids. By substituting diffusion coefficients obtained from MD simulation at corresponding lipid regions into the finite element simulation, we obtained results that matched the experimental data, validating the accuracy of our multiscale model. This model can serve as a predictor of experimental results, allowing for a better understanding of the penetration mechanism of drugs or cosmetics into the skin, ultimately leading to the optimization of their design and use to enhance their therapeutic or cosmetic effects.

https://doi.org/10.1021/acs.jpcb.4c00735
J. Phys. Chem. B 2024, 128, 6327−6337

2. MATERIALS AND METHODS

2.1. Materials. Mandelic acid (MAN, Aladdin M107076−100g; 99%), nicotinamide (NIC, Aladdin N105042−500g; 99%), pyruvic acid (PYR, Aladdin P104138−500g; 98%). Ultrapure water with a resistivity of 18.2 MΩ·cm, obtained from the Millipore Simplicity water purification system, was utilized as the solvent for all experiments conducted. All active ingredients were produced as a donor at 60 mg/mL concentration. Physiological saline was prepared from sodium chloride (Aladdin C111533−500g; 99.5%). Porcine dorsal skin was obtained from a slaughterhouse and stored in the freezer at −20 °C.

2.2. Methods. *2.2.1. Transdermal Behavior Studies. 2.2.1.1. Franz Cell Test.* The transdermal behavior experiments were performed using porcine dorsal skin in Franz cells. Before transdermal experiments, the skin was cut to an appropriate size, soaked in physiological saline, and dried using filter paper. The skin then was fixed between the donor and receptor compartments in a Franz diffusion cell. 8.2 mL of physiological saline and a stir bar were added to the receptor compartment and a 2 mL solution of the active ingredient was applied to the donor compartment. The concentration of active ingredient solution was 60 mg/mL. The donor compartment faced the stratum corneum, and the receptor compartment faced the viable epidermis. The effective permeation area was 2.11 cm^2. After assembling the diffusion cell, it was stirred continuously at (37 ± 0.5) °C and 300 rpm, 0.4 mL of the receptor solution was withdrawn and an equal volume of physiological saline was added at 0.5, 1, 2, 4, 6, and 8 h.

2.2.1.2. Quantification of Active Ingredients. The active ingredients quantification was conducted using UV spectrophotometry (UV-2450 Shimadzu). We used MAN as an example to generate the standard curve. Precisely 8 mg of MAN was weighed and prepared as an 80 μg/mL reserve solution with a total volume of 100 mL. Then, 0.1, 0.3, 0.6, 0.8, and 1.1 mL of the reserve solution were diluted with ultrapure water to obtain five concentration gradient standard solutions ranging from 2 to 22 μg/mL. Ultrapure water was used as a reference solution, and the absorbance of each standard solution was measured at the maximum absorption wavelength. The standard curve was then plotted with the concentration of the standard solution on the x-axis and the absorbance on the y-axis. After linear regression, the regression equation was obtained with $R^2 = 0.999$. The standard curves, R-squared, and linear ranges of the three active ingredients are shown in Table 1.

Table 1. Standard Curves, R^2, and Linear Range of the Active Ingredients

	standard curve	R^2	linear range [mg/mL]
MAN	$y = 1.5257x + 9.96 \times 10^{-4}$	0.9999	0.02−0.4
NIC	$y = 25.116x - 0.00412$	0.9995	0.001−0.03
PYR	$y = 0.3095x + 0.00103$	0.9997	0.05−0.6

Based on the standard curves, the concentration of the receptor solution could be determined. We added ultrapure water to the receptor solution and diluted it to a total volume of 3.0 mL. The absorbance of the receiving solution was measured at the maximum absorption wavelength with ultrapure water as the reference solution.

2.2.1.3. Statistical Analysis. Based on experimental data, we can compute the in vitro permeation parameters of active ingredients, such as cumulative release, cumulative release rate, and permeability coefficient.

To calculate the cumulative release per unit area of the n-th sampling Q_n, formula 2 was used.

$$Q_n = \frac{C_n \cdot V + \sum_{i=1}^{n-1} C_i \cdot V_i}{S} \tag{2}$$

where C_n is the concentration (mg/mL) of the n-th sampling, V is the volume (mL) of the receiving solution, C_i is the concentration (mg/mL) of the i-th sampling, V_i is the volume (mL) of the i-th sampling, and S is the diffusion area (cm^2).

To calculate the percentage of cumulative release η, formula 3 was used.

$$\eta = \frac{Q_n}{Q} \times 100\% \tag{3}$$

where Q_n is the cumulative release per unit area of the n-th sampling (mg/cm^2) and Q is the active ingredient loading per unit area in the diffusion cell (mg/cm^2).

In the graph of the cumulative release of active ingredients over time, the intercept of the linearly fitted line with the x-axis represents the lag time T_{lag}, and the slope represents the steady-state flux J_{ss}. The permeability coefficient k_p can be calculated based on J_{ss}, where $k_p = J_{ss}/C_v$, where C_v represents the concentration of active ingredients in the diffusion cell. These parameters are obtained through linear regression analysis of the linear portion of the curve.

2.2.2. Molecular Dynamics Simulation. The transdermal behavior of three active ingredients in the stratum corneum was simulated by molecular dynamics. The lipid bilayer structure was generated using the genmixmem1.2[29] software, with FFA, CER[NS], and CHOL, comprising 42, 42, and 44 molecules, respectively, to ensure a molar ratio of approximately 1:1:1.[23] 3900 water molecules were added to the outer surface of the lipid bilayer and distributed evenly on both sides of the lipid bilayer. Three kinds of active ingredients of MAN, NIC, and PYR were added into the lipid bilayer, respectively. All MD simulations were performed with the GROMACS2018.8 package.[30] The force field parameters were taken from the CHARMM36 lipid force field, and the TIP3P model was used for water.[31−34] Figure 1 shows the lipid bilayer constructed in this work.

The simulation time step was set to 2 fs. A cutoff of 1.2 nm was used for van der Waals and electrostatic interactions. The long-range electrostatic interactions were handled by the particle-mesh Ewald (PME) method.[35] The LINCS algorithm constrains the bonds containing hydrogen atom.[36] The Verlet algorithm was used as an integrator of Newton's equation of motion.[37] The systems were equilibrated at 310 K for 100 ns in an NPT ensemble with a v-rescale thermostat[38] and a Berendsen barostat.[39] Then, the production MD runs were performed for 40 ns in the NPT ensemble with a v-rescale thermostat and semi-isotropic Parrinello−Rahman barostat.[40] The compressibility was set to 4.5×10^{-5} bar^{-1}.

2.2.2.1. Diffusion Coefficient of Active Ingredients. The active ingredients were constrained at the boundary or center region of the lipid bilayer. The z coordinate of the lipid bilayer center was defined to be 0, and the molecular center of mass coordinates in the lipid bilayer boundary region was ±2 nm.

https://doi.org/10.1021/acs.jpcb.4c00735
J. Phys. Chem. B 2024, 128, 6327−6337

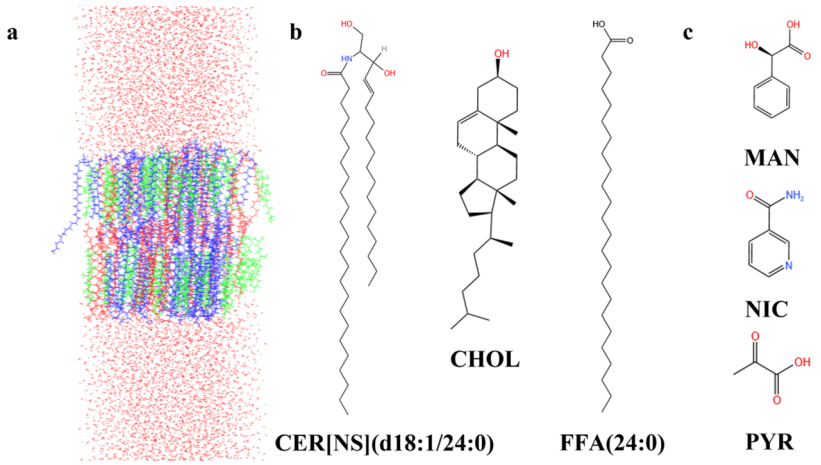

Figure 1. (a) Configuration of the lipid bilayer. CER[NS], CHOL, and FFA are shown in blue, green, and red, respectively. (b) Structural formulas of the three lipids that constitute the lipid bilayer. (c) Structural formulas of 3 kinds of active ingredients of MAN, NIC, and PYR.

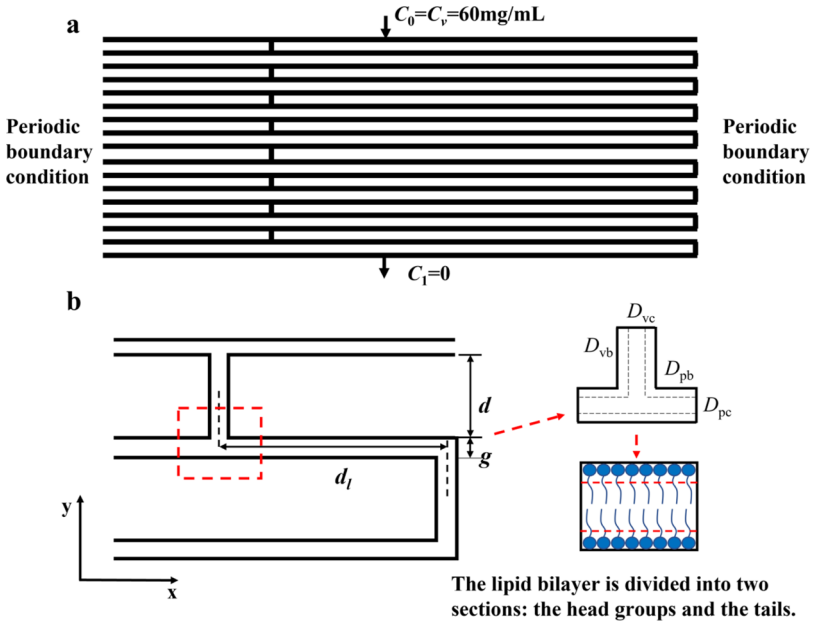

Figure 2. (a) Model of the stratum corneum containing lipid pathways, with periodic boundary conditions applied on the left and right sides of the model. The concentration of active ingredients at the top of the model is set at 60 mg/mL, while the concentration at the bottom outlet is set to 0. (b) A unit of the stratum corneum model, and the lipid pathway was divided into hydrophilic and hydrophobic microzones in a 1:4:1 ratio.

The lateral diffusion coefficients were calculated by the following formula:

$$D_{xy} = \lim_{t\to\infty} \frac{\langle |\boldsymbol{r}(t) - \boldsymbol{r}(0)|^2 \rangle}{2Nt} \quad (4)$$

where N is the dimension of the system (here N = 2), $\boldsymbol{r}(t)$ is the molecule's position at moment t, and $\langle\ \rangle$ denotes averaging over multiple molecules.

The random force applied to the molecule was recorded at the last 40 ns, and the autocorrelation function of the random force was calculated. The z-direction diffusion coefficient (D_z) was then calculated using the Kubo relation.[41,42]

$$D_z = \frac{(RT)^2}{\int_0^{+\infty} \delta F(z, t)\delta F(z, 0)\mathrm{d}t} \quad (5)$$

where δF (z_0, t) is the force autocorrelation function (fACF), R is the universal gas constant, and T is the temperature.

2.2.3. Finite Element Simulation. In this study, the diffusion behavior of MAN, NIC, and PYR in a stratum corneum model was investigated using finite element simulations by COMSOL Multiphysics 5.3. The structure and a unit of the two-dimensional model are shown in Figure 2.

The geometric parameters of the model are shown in Table 2. The offset ratio ω represents the ratio of the long and short paths of lipid lateral diffusion within a complete lateral diffusion path, $\omega = d_l/d_s$. The experiments demonstrate that the ω of mammals is usually around 3.[43] Therefore, the offset ratio of the model is set to 3.

The diffusion of active ingredients in the stratum corneum follows Fick's law. Here, Fick's law was solved in the finite element model using diffusion coefficients obtained from molecular dynamics simulations. The flux at the bottom over time was calculated, and the cumulative release was obtained

https://doi.org/10.1021/acs.jpcb.4c00735
J. Phys. Chem. B 2024, 128, 6327−6337

Table 2. Geometric Parameters of the Finite Element Model[44]

parameter	value
number of corneocyte layers, N	16
thickness of corneocytes, d	0.8 μm
length of corneocytes, l	40 μm
thickness of intercellular lipid, g	75 nm
long diffusion path,d_l	30.06 μm
short diffusion path,d_s	10.02 μm
offset ratio, ω	3

by integrating the flux. The expression of Fick's law is shown in formula 6.

$$\frac{\partial C(z,t)}{\partial t} = D\nabla^2 C(z,t) \tag{6}$$

where C is the concentration of active ingredients, t is time, and D is the diffusion coefficient of active ingredients within the intercellular lipids.

As the lipids between the cells form a multilayered structure, the lipid bilayers in the model were divided into three regions with a thickness ratio of 1:4:1, corresponding to the hydrophilic headgroup and the hydrophobic tail regions. The diffusion of active ingredients in the lipid bilayer is anisotropic, and the corresponding diffusion coefficients are given in formula 7.

$$D_{pb} = \begin{pmatrix} D_{bxy} & 0 \\ 0 & D_{bz} \end{pmatrix} D_{pc} = \begin{pmatrix} D_{cxy} & 0 \\ 0 & D_{cz} \end{pmatrix}$$
$$D_{vb} = \begin{pmatrix} D_{bz} & 0 \\ 0 & D_{bxy} \end{pmatrix} D_{vc} = \begin{pmatrix} D_{cz} & 0 \\ 0 & D_{cxy} \end{pmatrix} \tag{7}$$

where p denotes parallel, representing the lateral diffusion pathway; v denotes vertical, representing the longitudinal diffusion pathway; b denotes boundary, representing the ingredients in the hydrophilic headgroup region; and c denotes center, representing the ingredients in the hydrophobic tail chain region.

The bottom boundary condition is assumed to be a "sink condition",[45] where the concentration at the bottom ($C_1 = 0$ in Figure 2) is zero. This condition is designed to ensure that the active ingredients maintain a low concentration while passing through the skin, allowing for continuous permeation of the active ingredients into the body, thereby achieving effective delivery and avoiding the accumulation of the active ingredients within the skin. The research group of Barbero and Frasch,[15] Kushner,[13] and Gajula[25] have all utilized this model assumption and obtained favorable results. "Sink condition" is an important concept in the design and evaluation of transdermal delivery systems, ensuring that the active ingredients diffuse through the skin in a predictable and controllable way.

In addition to the bottom boundary condition, the model's other boundary conditions are also provided here. Concentration at the top of the model $C(z = L, t) = C_v$ mg/mL; the corneocyte-lipid boundary diffusion flux $J_{cl} = 0$; and periodic boundary conditions are applied on the left and right sides of the model.

By counting the diffusion flux and cumulative release at the bottom of the model, we can compare the results with those from experiments. Formulas 8 and 9 are the diffusion flux and cumulative release at the bottom of the model, respectively.

$$J = D\frac{\partial C(z,t)}{\partial z} \tag{8}$$

$$Q(t) = \int_0^t J(z=0,t)\mathrm{d}t = \int_0^t D\frac{\partial C(z=0,t)}{\partial z}\mathrm{d}t \tag{9}$$

To verify the accuracy of our model, we also calculated J_{ss} and T_{lag} for the three actives using Kushner's and Barbero and Frasch's models. In Kushner's model, J_{ss} and T_{lag} were calculated using formulas 10 and 11, respectively. And in Barbero and Frasch's model, we used their model, methodology, and some of their parameters for the calculations.

$$T_{lag} = \frac{\tau_{flux}\tau_{volume}L^2}{6D_b} \tag{10}$$

$$J_{ss}(z=0,t) = Q'(t) = \frac{\varepsilon K_b C_2 D_b}{\tau_{flux} L} \tag{11}$$

The parameters above are listed in Table 3.

3. RESULTS AND DISCUSSION

3.1. Transdermal Behavior of Active Ingredients. In vitro transdermal experiments on three active ingredients were conducted using a Franz cell. By using UV spectrophotometry to measure the concentration of the receptor solution and applying formula 2, the cumulative release was calculated. The $Q-t$ plots are presented in Figure 3. It shows the relationship between cumulative release over time for the three active ingredients. The order of cumulative release at the eighth hour from largest to smallest is PYR (3.24 mg/cm^2), MAN (2.48 mg/cm^2), and NIC (0.88 mg/cm^2). PYR has the largest cumulative release, while NIC has the lowest amount permeating through the skin.

Based on Figure 3, we calculated the cumulative release rate, lag time, and permeability coefficient, and the results are listed in Table 4. The linear portion of the cumulative release is used to calculate the steady-state flux J_{ss}, and the positive intercept with the x-axis represents the lag time T_{lag}. The permeability

Table 3. Parameters Used in Kushner's Model

parameters	definition	formula (if any)	note
τ_{flux}	flux of material through the thin slice of SC	$\tau_{flux} = \frac{Nh + (N-1)g + (N-1)\frac{\omega}{(1+\omega)^2}d}{Nh + (N-1)g}$	
τ_{volume}	total amount of lipids in the SC slice	$\tau_{flux} = \frac{Nh + (N-1)g + (N-1)d}{Nh + (N-1)g}$	
K_b	partition coefficient between donor and lipid		
C_2	donor concentration		
D_b	diffusion coefficient in lipid		$D_b = D_{cz}$ (we calculate)

https://doi.org/10.1021/acs.jpcb.4c00735
J. Phys. Chem. B 2024, 128, 6327−6337

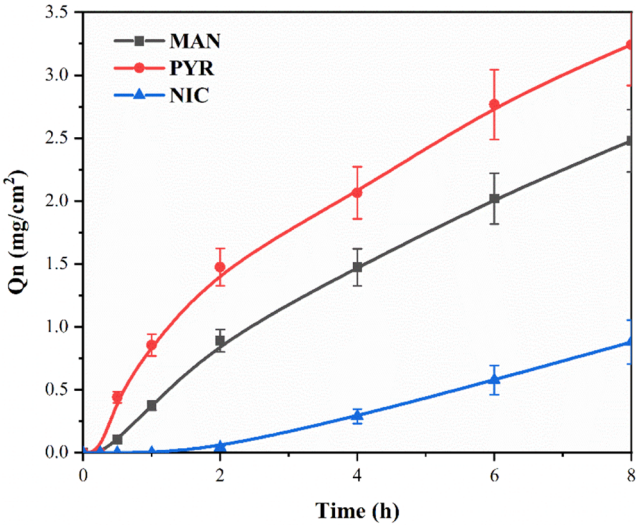

Figure 3. Cumulative release of each active ingredient over time.

Table 4. Cumulative Release Rate η, Steady-State Flux J_{ss}, Permeability Coefficient k_p, and Lag Time T_{lag} of Active Ingredients

	η [%]	J_{ss} [mg/cm² h]	k_p [cm/h]	T_{lag} [h]
MAN	4.36	0.513	8.55×10^{-3}	0.272
NIC	1.54	0.140	2.33×10^{-3}	1.81
PYR	5.70	1.095	1.82×10^{-2}	0.189

coefficient k_p reflects the ability of each ingredient to permeate the stratum corneum and is calculated as the ratio of steady-state flux to donor concentration. The cumulative release rate of NIC is 1.54, which is very small. This result is consistent with the literature,[46] proving the reliability of our experiments.

The order of cumulative release for the three ingredients is PYR > MAN > NIC, and the order of cumulative release rate, steady-state flux, and permeability coefficient is also the same. PYR shows the highest cumulative release rate of 5.70%, with J_{ss} = 1.095 mg/cm²h and k_p = 1.82 × 10^{-2} cm/h, demonstrating the strongest penetration ability. The results indicate that PYR is relatively easier to penetrate the stratum corneum, followed by MAN, and NIC has the weakest permeability.

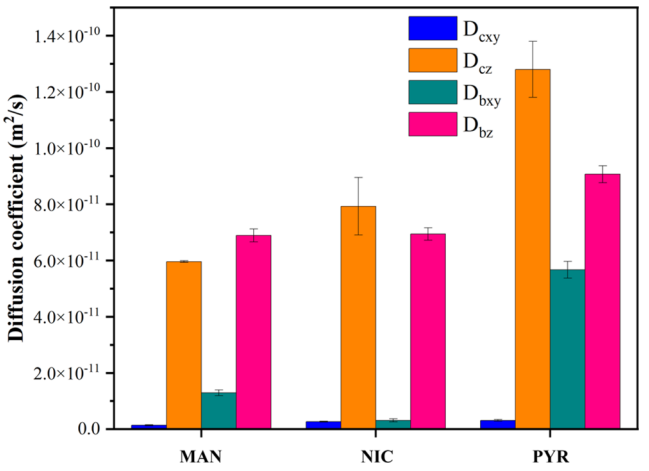

Figure 5. Diffusion coefficients of active ingredients in the center and boundary of the lipid bilayer, lateral and vertical, respectively

3.2. Molecular Dynamics Simulations of Active Ingredients within Lipid Bilayers. As the density distribution graphs of the three ingredients are similar, here we choose NIC as the illustrative ingredient. As shown in Figure 4, both CER and FFA are distributed throughout the SC membrane, while CHOL is mainly distributed in the outer layer, and FFA is mostly distributed in the inner layer for every system. This SC membrane structure is similar to the previous works.[22,47] The three active ingredients appear only in the center or the boundary, indicating that they are successfully constrained at the boundary or center region. In addition, the density differences of the components that make up the lipid bilayer are not substantial when active ingredients are placed at the edge or center of the lipid bilayer.

Here, we calculated the diffusion coefficients of different active ingredients at different positions within the lipid bilayer. The lateral (xy) diffusion coefficient was obtained by fitting the linear region of the MSD-t relationship. The vertical (z) diffusion coefficient was determined by analyzing the changes in the random forces on the ingredients in the z-direction and calculating the force autocorrelation function.

For each active ingredient, regardless of the boundary or central region of the lipid bilayer, its lateral diffusion coefficient D_{xy} is smaller than the vertical diffusion coefficient D_z,

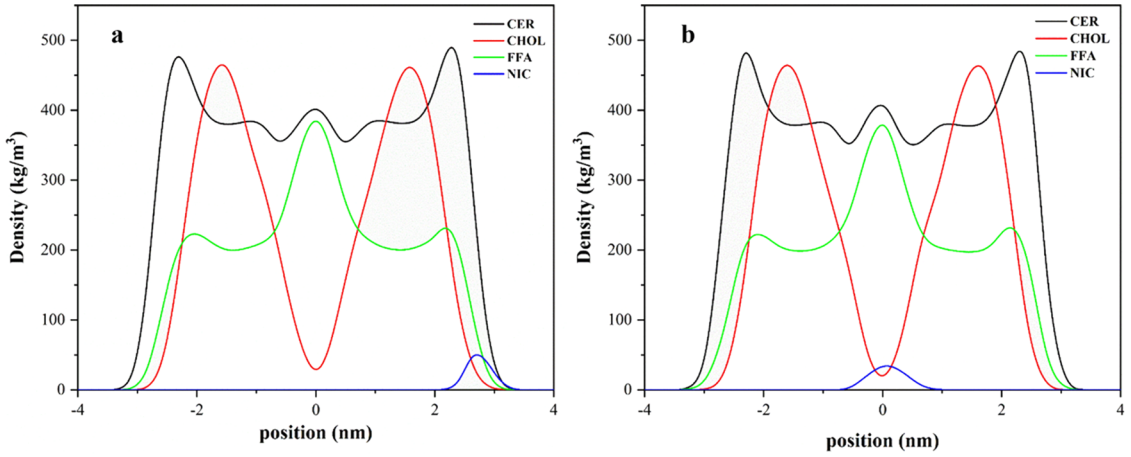

Figure 4. Density profile of each component of the lipid bilayer. (a) NIC at the boundary of the lipid bilayer. (b) NIC at the center of the lipid bilayer.

https://doi.org/10.1021/acs.jpcb.4c00735
J. Phys. Chem. B 2024, 128, 6327−6337

Table 5. Experiment and Simulation Results of In Vitro Permeation Parameters for Each Ingredient

	J_{ss} [mg/cm^2 h]		T_{lag} [h]		k_p [cm/h]	
	exp.	sim.	exp.	sim.	exp.	sim.
MAN	0.513 ± 0.103	0.2936	0.272 ± 0.135	1.43	$(8.55 \pm 1.72)\times10^{-3}$	4.89×10^{-3}
NIC	0.14 ± 0.03	0.1370	1.81 ± 0.23	2.42	$(2.33 \pm 0.50)\times10^{-3}$	2.28×10^{-3}
PYR	1.095 ± 0.219	1.191	0.189 ± 0.075	0.357	$(1.82 \pm 0.365)\times10^{-2}$	1.98×10^{-2}

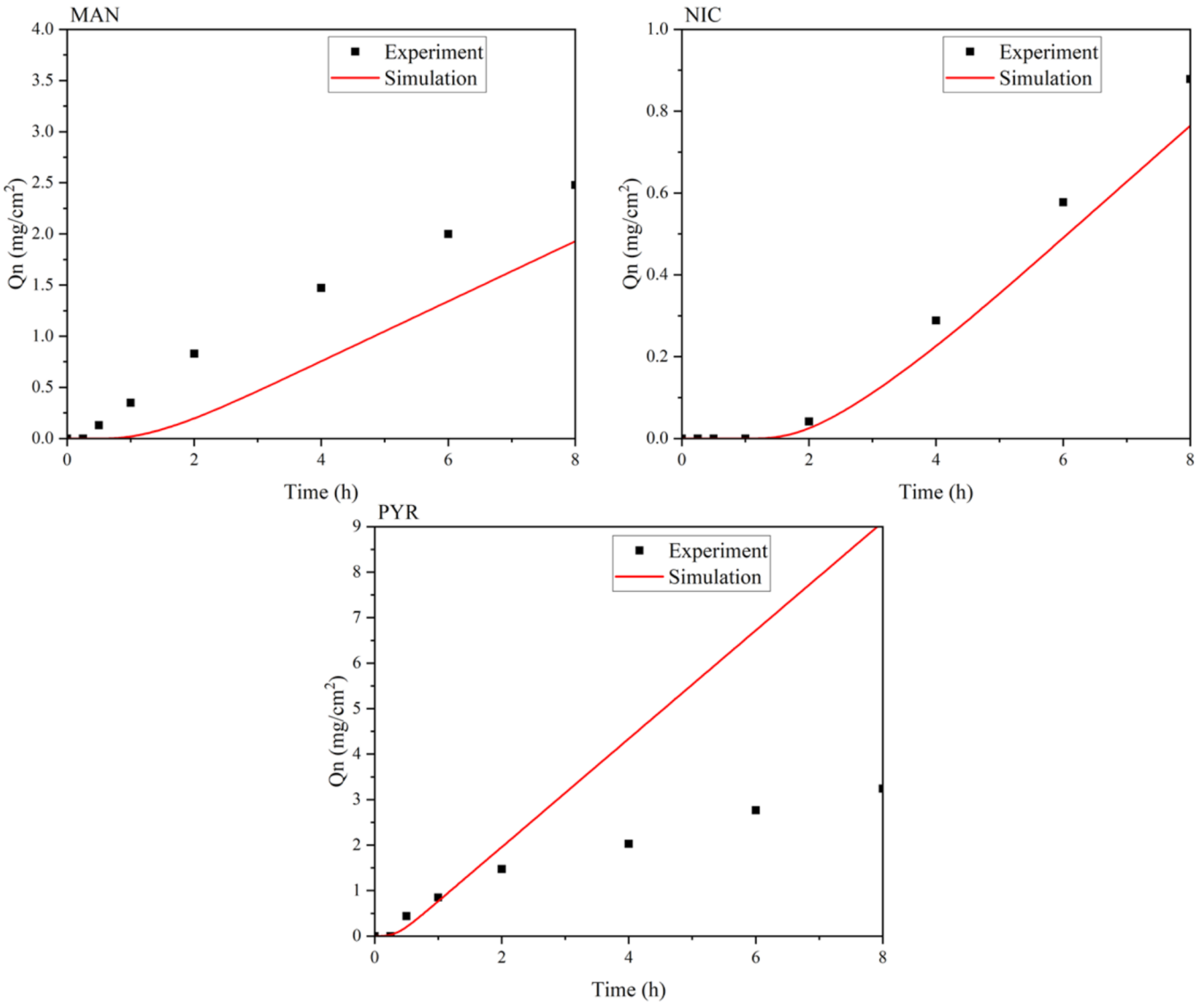

Figure 6. Cumulative release profile of MAN, NIC, and PYR through skin SC lipid region. FEM simulation vs experiments.

indicating that the active ingredient tends to diffuse vertically rather than laterally in the lipid bilayer. In addition, the lateral diffusion coefficient of these active ingredients in the central region of the lipid bilayer D_{cxy} is smaller than the lateral diffusion coefficient in the boundary region D_{bxy}. As the MW decreases, the diffusion coefficient of the active ingredients increase, which is consistent with the relationship between the diffusion coefficient and the MW obtained by Wang's research group.[16]

3.3. Diffusion Behavior of Active Ingredients in the Stratum Corneum. We utilized the diffusion coefficients obtained from molecular dynamics simulations into finite element simulations to calculate the in vitro permeation parameters of active ingredients in the stratum corneum, using formulas 8 and 9. By determining the slope of the linear portion and the positive intercept of the x-axis on the $Q-t$ plots, we obtained the steady-state flux and lag time, respectively. The comparison of simulation and experimental results is presented in Table 5.

We compared the simulation and experimental results of three active ingredients, MAN, PYR, and NIC. For J_{ss}, the simulation value of MAN is about 1/2 of the experimental result, while the simulation results of NIC with PYR are very close to the experimental results. For T_{lag}, the simulation results are all larger than the experimental ones, where the simulation results for NIC are close to the experimental data, and for MAN, it differs significantly from the experiment. Although there are differences between the simulation and

https://doi.org/10.1021/acs.jpcb.4c00735
J. Phys. Chem. B 2024, 128, 6327−6337

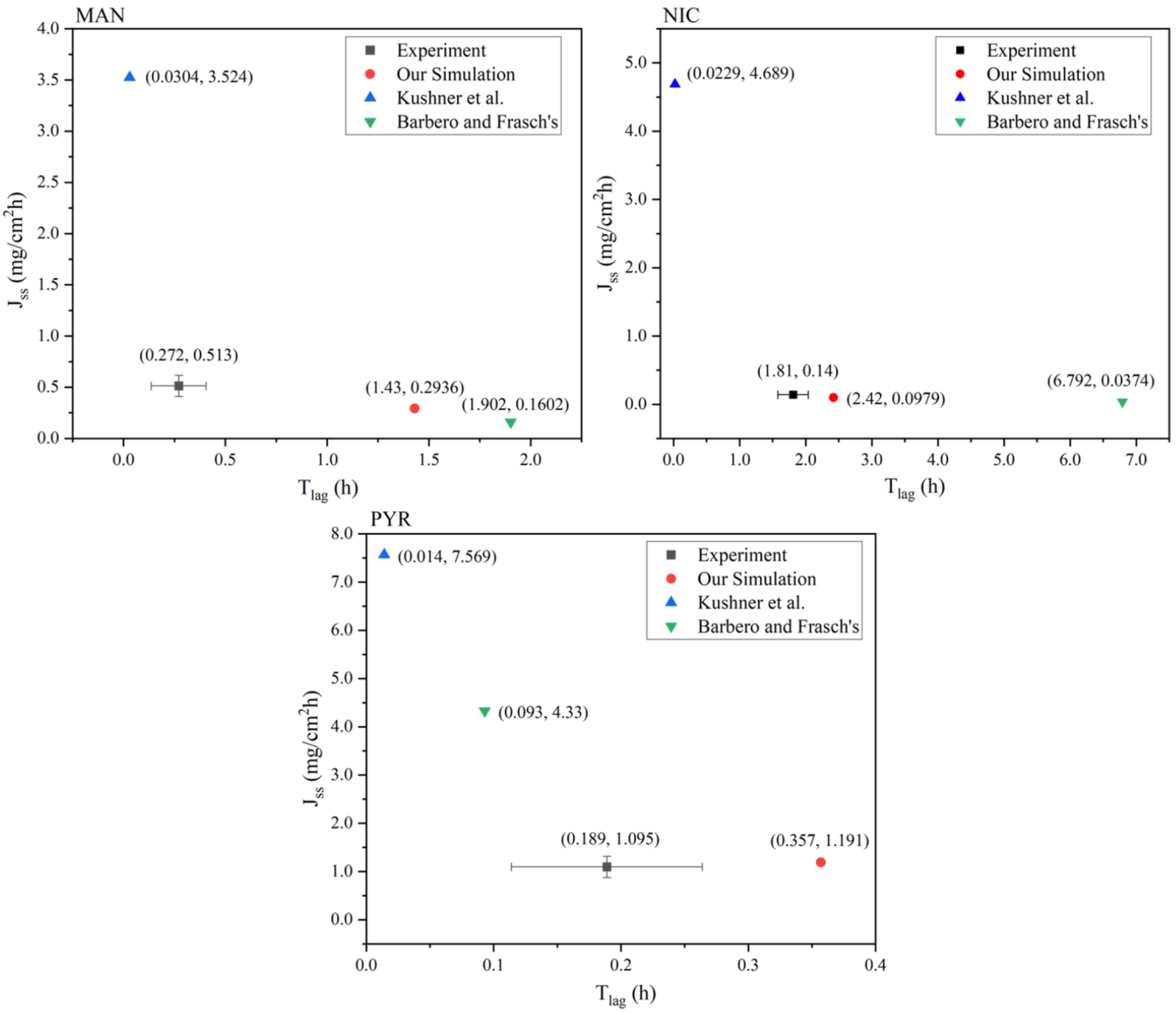

Figure 7. Distribution of J_{ss} and T_{lag} for the three active ingredients in different lipid model conditions.

experimental results, the order of magnitude is consistent: for J_{ss}, PYR > MAN > NIC, and for T_{lag}, NIC > MAN > PYR. The release profile is also compared in Figure 6, the experimental and simulation results exhibit minimal discrepancy. Hence, our model is more effective in predicting the transdermal behavior of these three active ingredients.

It is quite common to observe differences between simulation results and experimental values. For instance, Barbero and Frasch's team predicted the steady-state flux and lag time of caffeine permeation through the skin, which was about 5-fold higher than the experimental values, respectively.[15] Additionally, Guy's predictions of the permeability coefficients for limonene and linalool[48] were about 3 orders of magnitude higher than the experimental ones obtained by Almeida et al.[49] These discrepancies can be influenced by the assumptions of the models and the experimental conditions.

The results of steady-state flux J_{ss} could not only contrast the simulation results with the experimental data but also calculate the partition coefficient of each active ingredient between the donor and the stratum corneum. According to Fick's law, the steady-state flux for the diffusion of active ingredients in a homogeneous membrane is expressed as follows:

$$J_{ss} = \frac{KDC}{L} \tag{12}$$

where K represents the partition coefficient, D represents the diffusion coefficient within the homogeneous membrane, C represents the concentration in donor, and L represents the membrane's thickness. Although the stratum corneum model contains tortuous lipid pathways, it is also reasonable to homogenize the stratum corneum by distributing the lipid pathways throughout the whole stratum corneum to study the partition conditions since the model contains only the diffusion coefficients of the lipids.

In Figure 2, we set the partition coefficient between the donor and stratum corneum to 1 by equating the inflow concentration (C_0) with the donor concentration (C_v). Therefore, by dividing the experimental and simulated values of J_{ss}, a parameter can be obtained to qualitatively compare the partitioning ability of the active ingredients in the stratum corneum, which is called "partition factor". For MAN, NIC,

https://doi.org/10.1021/acs.jpcb.4c00735
J. Phys. Chem. B 2024, 128, 6327−6337

and PYR, the partition factors are 1.747, 1.022, and 0.919, respectively. Checking the octanol−water partition coefficients (log P) from PubMed (http://pubchem.ncbi.nlm.nih.gov/), we found log P values of 0.6, −0.4, and −0.5 for MAN, NIC, and PYR, respectively. It indicates that the lipophilicity ranking of the three species is as follows: MAN > NIC > PYR. Our model's partition factor order aligns with these values, showing that it accurately reflects the lipophilicity of the active ingredients seen in experimental data.

3.4. Effect of Different Lipid Model Conditions on Simulation Results. The diffusion conditions of ingredients in lipids are often set differently in different models of the stratum corneum. Kushner's team used an isotropic lipid model to derive the analytical solutions for J_{ss} and T_{lag}.[13] And in Barbero and Frasch's model, they used an anisotropic but unstratified lipid structure, and the lipid diffusion coefficients were obtained according to the empirical formulas.[15] In comparison, our model considered both the anisotropic lipid conditions and the stratification of lipids, thereby considering the diffusion behavior in different regions of the membrane. The comparison between the results of these three models and experimental data is presented in Figure 7.

For all three active ingredients, Kushner's isotropic model resulted in lower T_{lag} and significantly higher J_{ss}, failing to accurately reflect their diffusion behavior. Barbero and Frasch's model produced a noticeably longer T_{lag} and much lower J_{ss} than experiment values for MAN and NIC, but the opposite was observed for PYR. Our model demonstrated advantages over the aforementioned models in predicting J_{ss} and T_{lag}; however, for PYR, our predicted T_{lag} was about twice the experimental value, while Barbero and Frasch's model was half of the experimental value. Our model can more accurately predict the permeation behavior of these active ingredients.

4. CONCLUSIONS

In this study, we developed a multiscale stratum corneum model to describe the diffusion behavior of active ingredients within it and to predict the permeation properties. We initially performed in vitro transdermal experiments on three active ingredients using Franz diffusion cells to obtain the permeation parameters of the three ingredients and found that PYR had the strongest permeation ability through the stratum corneum, followed by MAN, and NIC had the weakest. We used molecular dynamics simulations to construct a lipid bilayer structure and obtained the diffusion coefficients of the active ingredients at the boundary and center region of the lipid bilayer. Our results showed that the active ingredients tended to diffuse vertically within the lipid bilayer. Subsequently, we developed a mesoscale model of the stratum corneum and used finite element simulation to calculate in vitro permeation parameters such as J_{ss} and T_{lag} of active ingredients. We also calculated the partition factor between the donor and stratum corneum. Our simulation results were compared to experimental data, and our model proved to be more accurate than other existing models. The constructed model successfully predicted the transdermal behavior of the active ingredients. This provides valuable insights into the penetration mechanism of drugs or cosmetics through the skin, allowing for the optimization of their design to enhance their therapeutic or cosmetic effects, as well as the ability to gain a better understanding of the skin's physiological state.

Generally, we successfully combined microscopic molecular dynamics simulations with mesoscopic finite element simulations to obtain parameters that can be compared with experimental results. The numerical values obtained by our model are in the same order of magnitude. They are numerically close to experimental results, demonstrating the potential of our model in predicting the transdermal behavior of active ingredients. However, it is important to acknowledge the limitations of our model. On the one hand, the accuracy of our model in predicting the transdermal behavior of more active ingredients remains to be validated. On the other hand, as the corneocytes in the stratum corneum undergo a process of maturation from the bottom to the top,[50] some of the corneocytes in the deeper layers may not be fully keratinized, which could increase the permeability of the deeper layers. Therefore, further research can be conducted to improve the model to predict the transdermal behavior of a more significant number of active ingredients.

■ ASSOCIATED CONTENT

Data Availability Statement

No data was used for the research described in the article.

■ AUTHOR INFORMATION

Corresponding Authors

Kangfu Zhou − *Yunnan Botanee Bio-Technology Group Co., Ltd., Kunming 650106, China*; Email: ericzhou@botanee.com

Yazhuo Shang − *Key Laboratory for Advanced Materials, School of Chemistry & Molecular Engineering, East China University of Science and Technology, Shanghai 200237, China*; orcid.org/0000-0003-1598-4711; Email: shangyazhuo@ecust.edu.cn

Authors

Qi Duan − *Key Laboratory for Advanced Materials, School of Chemistry & Molecular Engineering, East China University of Science and Technology, Shanghai 200237, China*

Zhicheng Ye − *Key Laboratory for Advanced Materials, School of Chemistry & Molecular Engineering, East China University of Science and Technology, Shanghai 200237, China*

Feifei Wang − *Yunnan Botanee Bio-Technology Group Co., Ltd., Kunming 650106, China; Yunnan Characteristic Plant Extraction Laboratory, Yunnan Yunke Characteristic Plant Extraction Laboratory Co., Ltd., Kunming 650106, China*

Cheng Lian − *Key Laboratory for Advanced Materials, School of Chemistry & Molecular Engineering, East China University of Science and Technology, Shanghai 200237, China*; orcid.org/0000-0002-9016-832X

Honglai Liu − *Key Laboratory for Advanced Materials, School of Chemistry & Molecular Engineering, East China University of Science and Technology, Shanghai 200237, China*; orcid.org/0000-0002-5682-2295

Complete contact information is available at: https://pubs.acs.org/10.1021/acs.jpcb.4c00735

Author Contributions

[‖]Q.D. and Z.Y. contributed equally to this work. Q.D.: Conceptualization, methodology, validation, investigation, writing—original draft. Z.Y.: Conceptualization, methodology, writing—review and editing. K.Z.: Investigation. F.W.: Investigation. C.L.: Supervision. Y.S.: Supervision, resources, writing—review and editing. H.L.: Supervision.

https://doi.org/10.1021/acs.jpcb.4c00735
J. Phys. Chem. B 2024, 128, 6327−6337

Notes

The authors declare no competing financial interest.

■ ACKNOWLEDGMENTS

The authors acknowledge the financial support of this work by the National Natural Science Foundation of China (no. 22308094), the independent research fund of Yunnan Characteristic Plant Extraction Laboratory (2022YKZY006), and the Fundamental Research Funds for the Central Universities (222201717003, 2022ZFJH004).

■ REFERENCES

(1) Fujiwara, A.; Morifuji, M.; Kitade, M.; Kawahata, K.; Fukasawa, T.; Yamaji, T.; Itoh, H.; Kawashima, M. Age-Related and Seasonal Changes in Covalently Bound Ceramide Content in Forearm Stratum Corneum of Japanese Subjects: Determination of Molecular Species of Ceramides. *Arch. Dermatol. Res.* **2018**, *310*, 729−735.

(2) Czekalla, C.; Schönborn, K. H.; Lademann, J.; Meinke, M. C. Noninvasive Determination of Epidermal and Stratum Corneum Thickness in Vivo Using Two-Photon Microscopy and Optical Coherence Tomography: Impact of Body Area, Age, and Gender. *Skin Pharmacol. Phys.* **2019**, *32*, 142−150.

(3) Gorcea, M.; Lane, M. E.; Moore, D. J. Exploratory in Vivo Biophysical Studies of Stratum Corneum Lipid Organization in Human Face and Arm Skin. *Int. J. Pharm.* **2022**, *622*, No. 121887.

(4) Nakazawa, H.; Ohta, N.; Hatta, I. A Possible Regulation Mechanism of Water Content in Human Stratum Corneum Via Intercellular Lipid Matrix. *Chem. Phys. Lipids* **2012**, *165*, 238−243.

(5) dos Santos, L.; Téllez S, C. A.; Sousa, M. P. J.; Azoia, N. G.; Cavaco-Paulo, A. M.; Martin, A. A.; Favero, P. P. In Vivo Confocal Raman Spectroscopy and Molecular Dynamics Analysis of Penetration of Retinyl Acetate into Stratum Corneum. *Spectrochim. Acta, Part A* **2017**, *174*, 279−285.

(6) van Smeden, J.; Janssens, M.; Gooris, G. S.; Bouwstra, J. A. The Important Role of Stratum Corneum Lipids for the Cutaneous Barrier Function. *Biochim. Biophys. Acta, Mol. Cell Biol. Lipids* **2014**, *1841*, 295−313.

(7) Williams, A. C.; Barry, B. W.; Moghimi, H. A Lamellar Matrix Model for Stratum Corneum Intercellular Lipids. Ii. Effect of Geometry of the Stratum Corneum on Permeation of Model Drugs 5-Fluorouracil and Oestradiol. *Int. J. Pharm.* **1995**, *131*, 117−129, DOI: 10.1016/0378-5173(95)04306-3.

(8) Kim, J.-Y.; Im, J. E.; Lee, J. D.; Kim, K.-B. Analytical Method Development and Percutaneous Absorption of Propylidene Phthalide, a Cosmetic Ingredient. *J. Toxicol. Environ. Health, Part A* **2021**, *84*, 811−820.

(9) Degim, I. T.; Pugh, W. J.; Hadgraft, J. Skin Permeability Data: Anomalous Results. *Int. J. Pharm.* **1998**, *170*, 129−133.

(10) Todo, H. Transdermal Permeation of Drugs in Various Animal Species. *Pharmaceutics* **2017**, *9*, 33.

(11) Rahma, A.; Lane, M. E.; Sinkó, B. A Comparative Study of the In Vitro Permeation of 2-Phenoxyethanol in the Skin PAMPA Model and Mammalian Skin. *Int. J. Pharm.* **2023**, *635*, No. 122692.

(12) Roper, C. S.; Howes, D.; Blain, P. G.; Williams, F. M. Percutaneous Penetration of 2-Phenoxyethanol Through Rat and Human Skin. *Food Chem. Toxicol.* **1997**, *35*, 1009−1016.

(13) Kushner, J.; Deen, W.; Blankschtein, D.; Langer, R. First-Principles, Structure-Based Transdermal Transport Model to Evaluate Lipid Partition and Diffusion Coefficients of Hydrophobic Permeants Solely from Stratum Corneum Permeation Experiments. *J. Pharm. Sci.* **2007**, *96*, 3236−3251.

(14) Cronin, M. T. D.; Dearden, J. C.; Moss, G. P.; Murray-Dickson, G. Investigation of the Mechanism of Flux Across Human Skin in Vitro by Quantitative Structure−Permeability Relationships. *Eur. J. Pharm. Sci.* **1999**, *7*, 325−330.

(15) Barbero, A. M.; Frasch, H. F. Effect of Stratum Corneum Heterogeneity, Anisotropy, Asymmetry and Follicular Pathway on Transdermal Penetration. *J. Controlled Release* **2017**, *260*, 234−246.

(16) Wang, T.; Kasting, G. B.; Nitsche, J. M. A Multiphase Microscopic Diffusion Model for Stratum Corneum Permeability. Ii. Estimation of Physicochemical Parameters, and Application to a Large Permeability Database. *J. Pharm. Sci.* **2007**, *96*, 3024−3051.

(17) Venable, R. M.; Krämer, A.; Pastor, R. W. Molecular Dynamics Simulations of Membrane Permeability. *Chem. Rev.* **2019**, *119*, 5954−5997.

(18) Gupta, R.; Dwadasi, B. S.; Rai, B. Molecular Dynamics Simulation of Skin Lipids: Effect of Ceramide Chain Lengths on Bilayer Properties. *J. Phys. Chem. B* **2016**, *120*, 12536−12546.

(19) Wang, E.; Klauda, J. B. Models for the Stratum Corneum Lipid Matrix: Effects of Ceramide Concentration, Ceramide Hydroxylation, and Free Fatty Acid Protonation. *J. Phys. Chem. B* **2018**, *122*, 11996−12008.

(20) Li, Q.; Fang, H.; Dang, E.; Wang, G. The Role of Ceramides in Skin Homeostasis and Inflammatory Skin Diseases. *J. Dermatol. Sci.* **2020**, *97*, 2−8.

(21) Das, C.; Olmsted, P. D.; Noro, M. G. Water Permeation Through Stratum Corneum Lipid Bilayers from Atomistic Simulations. *Soft Matter* **2009**, *5*, 4549.

(22) Gupta, R.; Sridhar, D. B.; Rai, B. Molecular Dynamics Simulation Study of Permeation of Molecules Through Skin Lipid Bilayer. *J. Phys. Chem. B* **2016**, *120*, 8987−8996.

(23) Lundborg, M.; Wennberg, C. L.; Narangifard, A.; Lindahl, E.; Norlén, L. Predicting Drug Permeability Through Skin Using Molecular Dynamics Simulation. *J. Controlled Release* **2018**, *283*, 269−279.

(24) Rim, J. E.; Pinsky, P. M.; van Osdol, W. W. Using the Method of Homogenization to Calculate the Effective Diffusivity of the Stratum Corneum with Permeable Corneocytes. *J. Biomech.* **2008**, *41*, 788−796.

(25) Gajula, K.; Gupta, R.; Sridhar, D. B.; Rai, B. In-Silico Skin Model: A Multiscale Simulation Study of Drug Transport. *J. Chem. Inf. Model.* **2017**, *57*, 2027−2034.

(26) Zahoor, M.; Shafiq, S.; Ullah, H.; Sadiq, A.; Ullah, F. Isolation of quercetin and mandelic acid from Aesculus indica fruit and their biological activities. *BMC Biochem.* **2018**, *19*, 5.

(27) Camillo, L.; Gironi, L. C.; Esposto, E.; Zavattaro, E.; Savoia, P. Nicotinamide and calcipotriol counteract UVB-induced photoaging on primary human dermal fibroblasts. *J. Photochem. Photobiol.* **2022**, *12*, No. 100158.

(28) Liu, M.; Yu, W.; Fang, Y.; Zhou, H.; Liang, Y.; Huang, C.; Liu, H.; Zhao, G. Pyruvate and lactate based hydrogel film inhibits UV radiation-induced skin inflammation and oxidative stress. *Int. J. Pharm.* **2023**, *634*, No. 122697.

(29) Tian, L. genmixmem program. http://sobereva.com/245 (accessed December 8, 2022).

(30) Abraham, M. J.; Murtola, T.; Schulz, R.; Páll, S.; Smith, J. C.; Hess, B.; Lindahl, E. GROMACS: High performance molecular simulations through multi-level parallelism from laptops to supercomputers. *SoftwareX* **2015**, *1−2*, 19−25.

(31) Jorgensen, W. L.; Chandrasekhar, J.; Madura, J. D.; Impey, R. W.; Klein, M. L. Comparison of simple potential functions for simulating liquid water. *J. Chem. Phys.* **1983**, *79*, 926−935.

(32) Vanommeslaeghe, K.; Hatcher, E.; Acharya, C.; Kundu, S.; Zhong, S.; Shim, J.; Darian, E.; Guvench, O.; Lopes, P.; Vorobyov, I.; Mackerell, A. D., Jr. CHARMM general force field: A force field for drug-like molecules compatible with the CHARMM all-atom additive biological force fields. *J. Comput. Chem.* **2010**, *31*, 671−690.

(33) Klauda, J. B.; Venable, R. M.; Freites, J. A.; O'Connor, J. W.; Tobias, D. J.; Mondragon-Ramirez, C.; Vorobyov, I.; MacKerell, A. D., Jr.; Pastor, R. W. Update of the CHARMM All-Atom Additive Force Field for Lipids: Validation on Six Lipid Types. *J. Phys. Chem. B* **2010**, *114*, 7830−7843.

(34) Yu, W.; He, X.; Vanommeslaeghe, K.; MacKerell, A. D., Jr. Extension of the CHARMM general force field to sulfonyl-containing compounds and its utility in biomolecular simulations. *J. Comput. Chem.* **2012**, *33*, 2451−2468.

https://doi.org/10.1021/acs.jpcb.4c00735
J. Phys. Chem. B 2024, 128, 6327−6337

(35) Essmann, U.; Perera, L.; Berkowitz, M. L.; Darden, T.; Lee, H.; Pedersen, L. G. A smooth particle mesh Ewald method. *J. Chem. Phys.* **1995**, *103*, 8577−8593.
(36) Hess, B. P-LINCS: A Parallel Linear Constraint Solver for Molecular Simulation. *J. Chem. Theory Comput.* **2008**, *4*, 116−122.
(37) Grubmüller, H.; Heller, H.; Windemuth, A.; Schulten, K. Generalized Verlet Algorithm for Efficient Molecular Dynamics Simulations with Long-range Interactions. *Mol. Simul.* **1991**, *6*, 121−142.
(38) Bussi, G.; Donadio, D.; Parrinello, M. Canonical sampling through velocity rescaling. *J. Chem. Phys.* **2007**, *126*, No. 014101.
(39) Berendsen, H. J. C.; Postma, J. P. M.; van Gunsteren, W. F.; DiNola, A.; Haak, J. R. Molecular dynamics with coupling to an external bath. *J. Chem. Phys.* **1984**, *81*, 3684−3690.
(40) Parrinello, M.; Rahman, A. Polymorphic transitions in single crystals: A new molecular dynamics method. *J. Appl. Phys.* **1981**, *52*, 7182−7190.
(41) Gaalswyk, K.; Awoonor-Williams, E.; Rowley, C. N. Generalized Langevin Methods for Calculating Transmembrane Diffusivity. *J. Chem. Theory Comput* **2016**, *12*, 5609−5619.
(42) Piasentin, N.; Lian, G.; Cai, Q. Evaluation of Constrained and Restrained Molecular Dynamics Simulation Methods for Predicting Skin Lipid Permeability. *Acs Omega* **2021**, *6*, 35363−35374.
(43) Talreja, P. S.; Kasting, G. B.; Kleene, N. K.; Pickens, W. L.; Wang, T.-F. Visualization of the Lipid Barrier and Measurement of Lipid Pathlength in Human Stratum Corneum. *AAPS PharmSci.* **2001**, *3*, 48−56.
(44) Johnson, M. E.; Blankschtein, D.; Langer, R. Evaluation of Solute Permeation through the Stratum Corneum: Lateral Bilayer Diffusion as the Primary Transport Mechanism. *J. Pharm. Sci.* **1997**, *86*, 1162−1172.
(45) Calcutt, J. J.; Anissimov, Y. G. Physiologically Based Mathematical Modelling of Solute Transport Within the Epidermis and Dermis. *Int. J. Pharm.* **2019**, *569*, No. 118547.
(46) Kasting, G. B.; Miller, M. A.; Xu, L.; Yu, F.; Jaworska, J. In Vitro Human Skin Absorption of Solvent-deposited Solids: Niacinamide and Methyl Nicotinate. *J. Pharm. Sci.* **2022**, *111*, 727−733.
(47) Gupta, R.; Rai, B. Molecular Dynamics Simulation Study of Skin Lipids: Effects of the Molar Ratio of Individual Components Over a Wide Temperature Range. *J. Phys. Chem. B* **2015**, *119*, 11643−11655.
(48) Guy, R. H. Predicting the Rate and Extent of Fragrance Chemical Absorption into and Through the Skin. *Chem. Res. Toxicol.* **2010**, *23*, 864−870.
(49) Almeida, R. N.; Costa, P.; Pereira, J.; Cassel, E.; Rodrigues, A. E. Evaporation and Permeation of Fragrance Applied to the Skin. *Ind. Eng. Chem. Res.* **2019**, *58*, 9644−9650.
(50) Évora, A. S.; Adams, M. J.; Johnson, S. A.; Zhang, Z. Corneocytes: Relationship Between Structural and Biomechanical Properties. *Skin Pharmacol. Phys.* **2021**, *34*, 146−161.

https://doi.org/10.1021/acs.jpcb.4c00735
J. Phys. Chem. B 2024, 128, 6327−6337